# Integration and modification of photosystem I for bio-photovoltaics

Gordiichuk, Pavlo

# 3 Photo-physical properties of photosystem I inside solid-state solar cells

Biomimetic strategies attracted an alluring attention for solar energy conversion in recent research efforts. Physical principles of light harvesting and energy transfer found in photosynthesis were implemented into solar cells and photo-active natural biomacromolecules integrated into existing solar technologies. Here, the large multi-protein complex photosystem I (PSI), which is at the heart of light-dependent reactions in photosynthesis, was integrated into a bulk heterojunction (BJH) solid-state organic solar cell. Thereby, the BHJ serves as a novel biophysical tool to determine the photo-induced dipole and the orientation of PSI on a substrate surface. Moreover, our experiments demonstrated that photoactive megadalton-protein complexes like PSI are compatible with solution processing of organic solar cells.

Gordiichuk, P. I., Wetzelaer, G.-J. A. H., Rimmerman, D., Gruszka, A., de Vries, J. W., Saller, M., Gautier, D. A., Catarci, S., Pesce, D., Richter, S., Blom, P. W. M. and Herrmann, A. ***Advanced Materials***, 26, 4863–4869 (2014).

## 3.1 Introduction

Solar cell technology has undergone dramatic changes over time, producing a vast diversity of approaches for light-to-energy conversion. The transition from inorganic to organic photosensitive materials represents a significant milestone in solar cell evolution. Organic dye-sensitized solar cells (DSSCs) are fabricated by immobilizing Ru-based light-absorbing chelates on a meso-porous $TiO_2$ working electrode in a two-electrode system. When illuminated, the organic dye is elevated to an excited state and injects electrons into the working metal-oxide electrode while an electrolyte solution shuttles electrons from the counter electrode to the dye, providing the voltage gradient required to perform electrical work.[1, 2] Another important advance toward practical organic photovoltaic devices has been the realization of "plastic" solar cells, or bulk heterojunctions. The active layer of such devices is composed of a microphase-separated morphology consisting of a p-type semi-conducting polymer and an electron acceptor moiety.[3-5] In contrast to DSSCs, these organic solid state devices can potentially be fabricated at low cost by all-solution processing and printing technologies even on flexible substrates.

Most recently, biomimetic strategies inspired the plants and photosynthetic organisms have been utilized for solar energy conversion. Thereby, processes occurring during photosynthesis, such as dynamic self-repair, light harvesting and quantum effects have been integrated into man-made photovoltaic devices.[6-9] Similarly, proteins that enable the natural photosynthesis process are integrated into existing solar energy technologies.[10-12] One of the most frequently used photo-active building blocks for that purpose is the multi-protein complex photosystem I (PSI). PSI contains a large antenna system in which light is harvested by photosynthetic pigments that absorb at distinct wavelengths and funnel the excitation energy to the special pair of chlorophylls (P700), where charge separation takes place. The high-energy electron travels via the primary electron acceptors $A_0$ (Chl*a*), $A_1$ (phylloquinone), $F_X$, $F_A$ and $F_B$ ($Fe_4S_4$ clusters) within the complex to ferredoxin. From there, the excited electron can either follow the cyclic- or noncyclic phosphorylation pathway to form ATP and redox-equivalents, respectively, finally enabling carbohydrate production.[13] The redox cycle is completed by re-reduction of $P700^{+\bullet}$ by cytochrome $c_6$. PSI is characterized by internal quantum efficiency close to 100%, which is one of the reasons why it has been employed in bio-inspired solar-energy conversion systems. Towards this goal, various PSI immobilization strategies have been evaluated with respect to the photoelectric properties of surface-immobilized PSI complexes and isolated reaction centres.[14-20] PSI stabilized with peptide detergents showed long-term stability and functionality under dry conditions on solid surfaces.[21] Based on these findings bio-photovoltaic devices similar to DSSCs were fabricated by self-assembly of PSI on 3D nanostructured semiconductor electrodes using a liquid electrolyte as redox mediator.[22] However, this architecture requires the use of a bio-friendly electrolyte solution that must be confined and sealed. To the best of our knowledge, the realization of a full solid-state bio-photovoltaic device with the favourable characteristics of an organic bulk heterojunction remains elusive.

Here, we introduce the implementation of PSI in organic electronic devices that combine the ease of processing of organic semiconductors with the bio-photovoltaic activity of PSI. The devices enable us to characterize biophysical properties of the photosynthetic multi-protein complex like its orientation on a surface. Such properties can otherwise only be determined by single molecule experiments employing scanning probe microscopy techniques.

## 3.2 Immobilization of PSI on a metal oxide surface

For our study, PSI from the cyanobacterium *T. Elongatus* was employed (**Figure 3.1a**). This photosynthetic complex contains 96 chlorophylls and 22 carotinoids for light absorption and can exist as a trimer *in vivo* with an overall molecular mass $M_r$ of 1 068 kDa (**Figures 3.1b and 3.1c**).[23, 24]

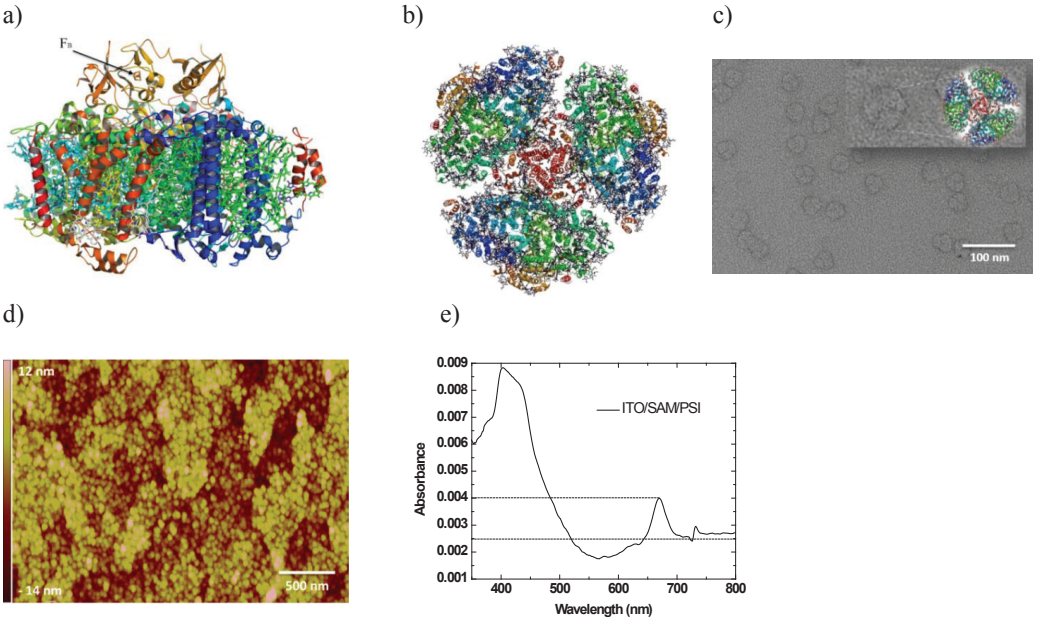


**Figure 3.1. (**a) Structure of a PSI monomer from *T. Elongatus* showing the polypeptide backbone and photosynthetic pigments.[24] (b) Structure of the trimer of PSI with a height of 6 nm and diameter of around 25 nm. (c) TEM image of PSI trimers employed for the preparation of solar cells. (d) AFM picture of a self-assembled monolayer of PSI trimers on an ITO surface measured in tapping mode. The substrate was pre-treated with dihydroxyacetone phosphate for adsorption of PSI. (e) Visible absorption spectra of a self-assembled monolayer of PSI on a ITO surface that was treated with dihydroxyacetone phosphate.

After purification of the trimeric protein complex (see Experimental section), a dense PSI monolayer was prepared in two steps on transparent metal oxide substrates. First, a self-assembled monolayer of dihydroxyacetone phosphate was established on indium-tin oxide (ITO) supported on glass substrates.[25] In the second step, the metal oxide surfaces were immersed in a

PSI solution. As a result, a dense monolayer of PSI was formed, as evidenced by AFM measurements (**Figure 3.1d and 3.2**). Counting of the PSI trimers on ITO was performed on different areas and revealed an average number of $1.7\times10^{15}$ $m^{-2}$ PSI monomers corresponding to a surface coverage of 50%. This high coverage allowed recording of an absorption spectrum of a PSI monolayer assembled on the transparent substrates under dry conditions, where the characteristic absorption peaks of PSI were detected at 430 and 660 nm (**Figure 3.1e**). These measurements indicate that the dihydroxyacetone phosphate linker is well suited for immobilization of PSI by binding to the metal-oxide surface and interacting with the polar stroma and lumen faces of PSI by electrostatic and hydrogen bonds.

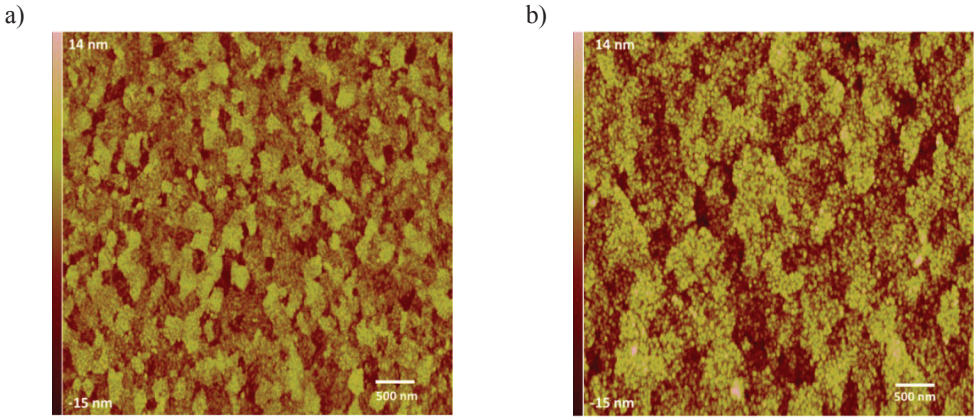


**Figure 3.2.** AFM height profile of ITO surface used for device fabrication before (a) and after (b) PSI immobilization. The z-scale is represented as colour code on the left of each picture with a range of 29 nm.

## 3.3 PSI stability study under organic solvent treatment

For incorporation of PSI into organic BHJs, it needs to be tested whether the biomacromolecular complex is compatible with the fabrication process. The effect of the organic solvent chlorobenzene on PSI structure and its surface coverage was studied with the help of AFM. PSI was immobilized in a similar way on a gold surface prepared by the template stripping method with the directing linker molecule 2-mercapto ethanol (concentration 1 mM in ethanol) by incubation for 12 h [26]. The hydroxyl groups introduced in this way induce a good PSI coverage after 2 h immobilization time in the dark (**Figure 3.3a**). The AFM measurements in tapping mode were recorded before and after spin-coating of 200 µL chlorobenzene solution on top of PSI monolayer at 2000 RPM speed and accelerating 2000 RPM/s (**Figures 3.3a and 3.3b**). The heights of PSI complexes in an imaging area of 1.5 by 1.5 µm were measured manually and plotted as height histograms shown in **Figures 3.3c** and **3.3d**. The organic solvent treatment induces a minor height reduction of PSI of less than 0.5 nm. Moreover, the spin coating of chlorobenzene results in decreasing surface coverage of PSI by 18% compared to the non-treated

area. From these measurements, it can be concluded that the most of PSI trimers on the surface remain structurally unaffected by the short treatment with organic solvent.

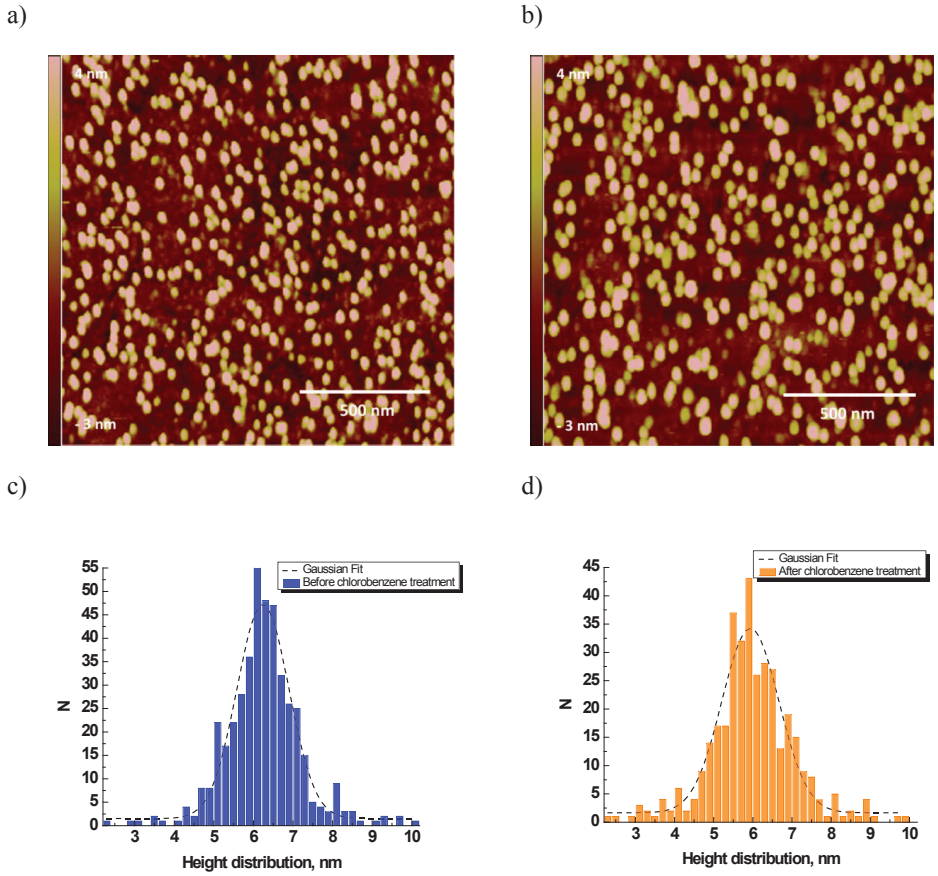


**Figure 3.3**. The PSI protein complexes denaturation on a gold surface under chlorobenzene treatment studied by AFM. (a) The height profiles with corresponding height histograms (c) of a fabricated PSI film before treatment. (b) The height profile of a PSI film after 1 time spin coating of chlorobenzene solvent with corresponding (d) height histogram.

## 3.4 Fabrication BJH solar cells with PSI monolayer

After demonstrating that PSI from thermophilic origin resists short organic solvent treatment, PSI was integrated into a solution processed organic semiconductor device. The incorporation of PSI in such devices is motivated by revealing the photo-induced dipole behaviour of PSI and to determine the orientation of PSI on the surface. To address these questions, PSI was introduced

into polymer-fullerene bulk heterojunctions (BHJs). A 1:4 mixture (by wt.) of the conjugated polymer MEH-PPV and the fullerene derivative PCBM dissolved in chlorobenzene were spin-coated on top of the dense monolayer of PSI on ITO.

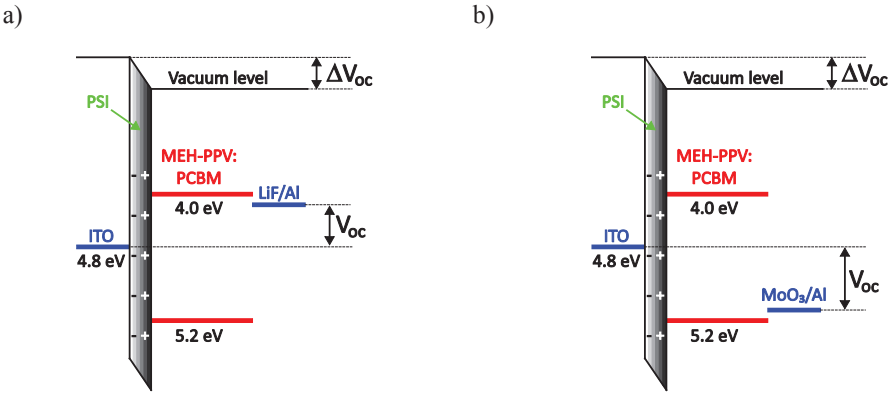


**Figure 3.4.** Energy diagrams of bulk heterojunctions containing a PSI electrode-modification layer. PSI is represented as an oriented dipole with corresponding shifts in $V_{OC}$. (a) The conventional solar-cell structure with LiF/Al as a top electrode. (b) Inverted device structure with $MoO_3$/Al as a top electrode.

In the final step of device fabrication, either electron-extracting (LiF/Al) or hole-extracting ($MoO_3$/Al) top electrodes were deposited atop the MEH-PPV layer by thermal evaporation with the corresponding energetic diagrams described in **Figure 3.4**. As a result, two types of cells were obtained, characterized by the flow of photogenerated current in opposite directions. In such devices, the current is mainly generated in the 120 nm thick organic BHJ, which absorbs substantially more light than the PSI monolayer. In this way, the PSI layer acts as modifier of the electrode allowing to extract photoelectric properties of the multiprotein complex. It is well known that the open-circuit voltage $V_{OC}$ of an organic BHJ solar cell is proportional to the difference in work function of the electrodes with and without PSI film.[27] In the PSI monolayer under illumination, electrons are directed to the acceptor side ($F_B$-$Fe_4S_4$ cluster) while positive charges (holes) remain at the P700 donor. This creates a dipole between the ITO and the organic BHJ, effectively modifying the work function of the ITO.[28] Since the open-circuit voltage depends on the work function difference between the ITO and the top electrode, the dipole orientation can be extracted.

As shown in **Figure 3.5**, the open-circuit voltage is lowered upon insertion of a PSI layer in the device with the low work function LiF/Al top electrode, whereas it increases in the cell with the high work function $MoO_3$/Al top electrode. This behaviour implies that the work function of ITO is decreasing by incorporation of the protein monolayer, indicating that the majority of the dipoles in the PSI layer are directed with the iron-sulphur cluster $F_B$ towards the ITO (compare **Figures 3.1a and 3.4**). In such an orientation the photo-generated electrons of PSI are predominantly expelled towards the metal oxide. The obtained solar cell parameters are summarized in **Table**

**3.1**. The data show that the incorporation of PSI has a significant effect on the open-circuit voltage while the other parameters are less affected.

a) b)

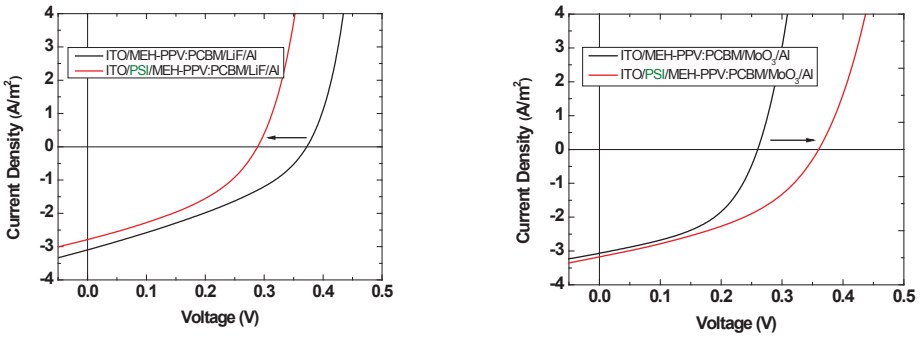


**Figure 3.5.** *J-V* curves of bulk-heterojunction solar cells under simulated sunlight with and without PSI. (a) Conventional device with ITO anode and LiF/Al cathode and (b) inverted device with ITO cathode and $MoO_3$/Al anode. Arrows indicate the shift in $V_{OC}$ due to the PSI modification layer, *i.e.*, work-function decrease of the bottom electrode. A neutral density filter with a transmission of 0.089 was used, resulting in an incident light intensity of about 89 W/m$^2$.

**Table 3.1.** Device characteristics of bulk-heterojunction solar cells with sandwich-type structures of ITO/MEH-PPV:PCBM and ITO/PSI/MEH-PPV:PCBM containing different top electrodes.

| Bottom electrode | Top Electrode | $V_{OC}$ (V) | $J_{SC}$, (A/m$^2$) | FF (-) | $\Delta V_{OC}$ (V) |
|---|---|---|---|---|---|
| ITO | LiF/Al | 0.39±0.02 | 3.09±0.01 | 0.41±0.08 | |
| ITO/PSI | LiF/Al | 0.34±0.05 | 2.81±0.17 | 0.41±0.02 | -0.05 |
| ITO | $MoO_3$/Al | 0.23±0.03 | 2.95±0.12 | 0.47±0.02 | |
| ITO/PSI | $MoO_3$/Al | 0.34±0.02 | 3.05±0.12 | 0.40±0.04 | +0.11 |

## 3.5 PSI dipole calculation

The shift in the work function due to PSI incorporation can be used to calculate surface charges using a simple capacitor model. As indicated before, the change in the $V_{OC}$ originates from a potential drop due to the dipole created by the charge separation in the PSI monolayer. Effectively, one can treat the PSI monolayer as a parallel-plate capacitor with capacitance $C = \varepsilon_r\varepsilon_0 A/L$, where $\varepsilon_0$ is the vacuum permittivity, $\varepsilon_r$ the relative permittivity, $A$ the surface area,

and $L$ the layer thickness. The total surface charge can now be calculated as $Q = C\Delta V_{OC}$, resulting in a surface charge density, $Q/eA$, of $1.84\times10^{15}$ $m^{-2}$, with $e$ the elementary charge, $\varepsilon_r = 4$, $\Delta V_{OC}$ = 0.05 V, and a thickness of a monolayer, $L$ = 6 nm. The value for the surface-charge density compares very well with the density of PSI on the ITO substrate determined by AFM ($1.7\times10^{15}$ $m^{-2}$), indicating that indeed PSI is mainly oriented with the $F_B$-$Fe_4S_4$ cluster pointing towards the metal oxide surface. In the next step, the dipole moment of PSI was calculated. Therefore, we used equation 1:

$$\Delta\varphi = \frac{N\mu\cos\theta}{\epsilon\epsilon_0}, \tag{1}$$

where $N$ is the number of absorbed molecules per surface area, μ is the dipole moment created with PSI, $\theta$ is the angle of dipole tilting on ITO, $\epsilon$ and $\epsilon_0$ are the dielectric constants of the monolayer and dielectric permittivity of vacuum respectively. Formula 1 can be rewritten in the following way expressing the PSI dipole moment $\mu_{PSI}$ as:

$$\mu_{PSI} = \frac{\varepsilon_0\varepsilon\,\Delta V_{oc}}{N}\ (2)\ (\text{suppose } \Delta V_{oc}\sim\Delta\varphi). \tag{2}$$

Thereby, it was assumed that $\Delta V_{OC}$ linearly depends on $\Delta\varphi$. As a result we obtained a value for $\mu_{PSI}$ of 295 D as calculated for $\Delta V_{OC}$ of the conventional device configuration. The dipole of PSI was calculated by theoretical model and estimated to be up to 1000 D[29]. The difference to our calue might be due to the fact that not all PSI trimers were oriented in the same direction. The effect of dipoles on $V_{OC}$ inside organic solar cells has been exhaustively studied before.[28, 30] These measurements demonstrate the compatibility of functional multiprotein complexes with organic electronic materials and existing processing strategies in this field like spin coating. Previously, dipole properties of proteins were measured by electric dichroism.[31] Here, we present an alternative strategy of assessing the dipole characteristics of PSI that qualities organic electronic devices as a new biophysical tool.

## 3.6 Conclusions

We successfully incorporated large photosynthetic complex trimers with an overall molecular weight of more than 1 000 kDa into bulk heterojunction solar cells that were exclusively prepared by solution processing. It was demonstrated that the biological component and organic semiconducting materials can be integrated without compromising their original optoelectronic properties. Spin coating a blend of donor and acceptor materials dissolved in an organic solvent did not affect the structural integrity of the photoactive protein complex. The type of device described herein represents a new biophysical tool allowing to study the dipole properties by measuring open circuit voltage shifts in conventional and inverted device configuration geometries. From the dipole characteristics, the orientation of PSI trimers on the surface was calculated, which is important for the fabrication of bioelectronic devices wherein PSI is the only photoactive component. Moreover, the devices described here might be employed in the future to

determine the dipole characteristics of other proteins as long as those are compatible with device fabrication conditions.

## 3.7 Methods

*Cell growth*: The thermophilic cyanobacterium *T. Elongatus BP1* (generous gift from M. Rögner, Ruhruniversität Bochum, Germany) was grown under agitation (150 rpm) in BG11 medium.[32] The temperature was kept at 56°C, continuous light applied at 50-60 μEinstein·$m^{-2}$·$s^{-1}$ and cell growth pursued until late log phase. At last, the cells were harvested by centrifugation [JLA 9.100 rotor, Beckman; 7500 g; 15 min], re-suspended in Buffer A [20 mM HEPES (pH 7.5); 10 mM $MgCl_2$; 10 mM $CaCl_2$; 500 mM Mannitol], snap-frozen in liquid nitrogen and stored at - 80°C.

*Thylakoid membrane preparation*: Thylakoid membranes were prepared according to the following protocol, which represents a combination of two previously described preparation methods.[33, 34] To this end, fresh or frozen cells were re-suspended in Buffer A and homogenized five times using a Dounce homogenizer. After the addition of lysozyme [final concentration: 0,5% (wt/vol)] and a tip of a spatula of DNase, the cell suspension was incubated under slow agitation for 45 min at 37°C in the dark. Subsequently, the cells were lysed by two passages through a French Press (15000psi; Constant Systems Limited, UK). Membranes were collected by centrifugation [JLA 16.250 rotor, Beckman; 38000 g; 20 min] and washed with Buffer A containing 3 M NaBr. Afterwards, the membrane suspension was washed once with Buffer A and three times with a buffer containing 0,05% DDM (n-Dodecyl-β-D-maltoside) in order to remove the phycobilisomes. Finally, the thylakoid membranes were solubilized by incubation in Buffer A and supplemented with 0,6% DDM for 30 min at 20°C in the dark. Non-solubilized material was pelleted by centrifugation [JLA 16.250 rotor, Beckman; 16000rpm (38000 g); 20 min] and the supernatant was subjected to subsequent purification steps.

*Photosystem I purification*: For PSI purification, fast liquid protein chromatography was applied on solubilized thylakoid membranes. The chromatographic purification was performed on a ÄKTA explorer [GE Healthcare] using an anion exchange column [HiTrapTM Q HP, GE Healthcare]. After column equilibration with Buffer A + 0,03% DDM, the sample was applied and subsequently eluted by a linear gradient of [0-1M] $MgSO_4$. The green fluorescent fractions were collected and desalted with Buffer A + 0,03% DDM using Vivaspin 20 columns [molecular weight cut-off: 100 kDa; GE Healthcare]. Finally, the purified PSI sample was adjusted to a Chl a concentration of 800 μM [with Buffer A + 0,03% DDM], snap-frozen in liquid nitrogen and stored at -80°C.

*Determination of chlorophyll a and protein concentration*: Chl a determination was performed in 100% methanol as described in Porra et al.[35]

*PSI immobilization on ITO surfaces and absorption spectrum measurements*: ITO surfaces were immersed overnight (14 hours) in 1 mM solution of dihydroxyacetone phosphate hemimagnesium

salt hydrate in deionized (DI) water. After washing the surfaces with DI water and drying with a flow of nitrogen, the substrates were ready for formation of PSI monolayers. Therefore, PSI stock solution was diluted twice with Buffer A and the substrates were incubated for 2 hours with this solution in the dark. After the immobilization, PSI substrates were rinsed with DI water and dried with a nitrogen flow. ITO substrates equipped with a PSI layer were used for device preparation. Absorption spectra of PSI monolayers were recorded with a Jasco V-630 spectrophotometer at 25°C under dry conditions. PSI ITO substrates were used for atomic force microscope (AFM) investigations and to assess the protein coverage.

*AFM measuremenrts*: Images were recorded in tapping mode by a Multimode 8 instrument with ScanAsyst, Controller V [Bruker]. The TESP silicon probe, 42 N/m spring constant, 320 kHz resonance frequency with tip radius of less than 10 nm was used for all measurements. Analysis of recorded height images was performed with NanoScopeAnalysis 1.2 software.

*Fabrication of photovoltaic device*: Glass substrates, pre-patterned with indium tin oxide, were thoroughly cleaned by washing with detergent solution, ultrasonication in acetone and isopropyl alcohol, followed by UV-ozone treatment. PSI protein were self-assemble on the surface. Subsequently, a 90 nm PTAA layer was spun from a chlorobenzene solution in a nitrogen-filled glovebox. The devices were finished by thermal evaporation of a $MoO_3$(10 nm)/Al(100 nm) top electrode at a base pressure of $1\times10^{-6}$ mbar. For the devices with a MEH-PPV:PCBM layer, the $TiO_x$ layer was omitted. The 120 nm MEH-PPV:PCBM (1:4 by wt.) layer was spin cast from a chlorobenzene solution. Top electrodes, $MoO_3$(10 nm)/Al(100 nm) or LiF(1 nm)/Al(100 nm) were thermally evaporated.

*Device characterization*: Electrical measurements were conducted in a controlled nitrogen atmosphere in the dark and under illumination of a Steuernagel Solar Constant 1200 metal halide lamp, which was set to 1 Sun intensity using a silicon reference cell and correcting for spectral mismatch. EQE spectra were recorded versus a silicon reference, using a custom-built setup comprising a lock-in amplifier, a transimpedance amplifier, and a focused, chopped monochromatic beam from a quartz tungsten halogen lamp, and a range of narrow band pass filters.

## 3.8 References


1. Gratzel, M. Photoelectrochemical cells. *Nature* **414**, 338-344 (2001).

2. Chung, I., Lee, B., He, J.Q., Chang, R.P.H. & Kanatzidis, M.G. All-solid-state dye-sensitized solar cells with high efficiency. *Nature* **485**, 486-U494 (2012).

3. Halls, J.J.M. et al. Efficient Photodiodes from Interpenetrating Polymer Networks. *Nature* **376**, 498-500 (1995).

4. Brabec, C.J., Sariciftci, N.S. & Hummelen, J.C. Plastic solar cells. *Adv. Funct. Mater.* **11**, 15-26 (2001).

5. Yu, G., Gao, J., Hummelen, J.C., Wudl, F. & Heeger, A.J. Polymer Photovoltaic Cells - Enhanced Efficiencies Via a Network of Internal Donor-Acceptor Heterojunctions. *Science* **270**, 1789-1791 (1995).

6. Ham, M.H. et al. Photoelectrochemical complexes for solar energy conversion that chemically and autonomously regenerate. *Nat. Chem.* **2**, 929-936 (2010).

7. Huang, J.S. et al. Polymer bulk heterojunction solar cells employing Forster resonance energy transfer. *Nat. Photonics.* **7**, 480-486 (2013).

8. Weil, T., Reuther, E. & Mullen, K. Shape-persistent, fluorescent polyphenylene dyads and a triad for efficient vectorial transduction of excitation energy. *Angewandte Chemie* **41**, 1900-1904 (2002).

9. Hayes, D., Griffin, G.B. & Engel, G.S. Engineering coherence among excited states in synthetic heterodimer systems. *Science* **340**, 1431-1434 (2013).

10. Yehezkeli, O. et al. Integrated photosystem II-based photo-bioelectrochemical cells. *Nat. Commun.* **3** (2012).

11. Krassen, H. et al. Photosynthetic Hydrogen Production by a Hybrid Complex of Photosystem I and [NiFe]-Hydrogenase. *ACS Nano* **3**, 4055-4061 (2009).

12. Iwuchukwu, I.J. et al. Self-organized photosynthetic nanoparticle for cell-free hydrogen production. *Nat. Nanotechnol.* **5**, 73-79 (2010).

13. Brettel, K. Electron transfer and arrangement of the redox cofactors in photosystem I. *BBA-Bioenergetics* **1318**, 322-373 (1997).

14. Blankenship, R.E. et al. Comparing Photosynthetic and Photovoltaic Efficiencies and Recognizing the Potential for Improvement. *Science* **332**, 805-809 (2011).

15. Das, R. et al. Integration of photosynthetic protein molecular complexes in solid-state electronic devices. *Nano Lett.***4**, 1079-1083 (2004).

16. Gerster, D. et al. Photocurrent of a single photosynthetic protein. *Nat.Nanotechnol.* **7**, 673-676 (2012).

17. Lee, I., Lee, J.W. & Greenbaum, E. Biomolecular electronics: Vectorial arrays of photosynthetic reaction centers. *Phys. Rev. Lett.* **79**, 3294-3297 (1997).

18. Trammell, S.A., Spano, A., Price, R. & Lebedev, N. Effect of protein orientation on electron transfer between photosynthetic reaction centers and carbon electrodes. *Biosens. Bioelectron.* **21**, 1023-1028 (2006).

19. Trammell, S.A., Wang, L.Y., Zullo, J.M., Shashidhar, R. & Lebedev, N. Orientated binding of photosynthetic reaction centers on gold using Ni-NTA self-assembled monolayers. *Biosens. Bioelectron.* **19**, 1649-1655 (2004).

20. Carmeli, I., Frolov, L., Carmeli, C. & Richter, S. Photovoltaic activity of photosystem I-based self-assembled monolayer. *J. Am. Chem. Soc.* **129**, 12352 (2007).

21. Kiley, P. et al. Self-assembling peptide detergents stabilize isolated photosystem I on a dry surface for an extended time. *Plos Biol.* **3**, 1180-1186 (2005).

22. Mershin, A. et al. Self-assembled photosystem-I biophotovoltaics on nanostructured TiO2 and ZnO. *Sci. Rep.* **2** (2012).

23. Boekema, E.J. et al. Evidence for a Trimeric Organization of the Photosystem-I Complex from the Thermophilic Cyanobacterium Synechococcus Sp. *FEBS Lett.* **217**, 283-286 (1987).

24. Jordan, P. et al. Three-dimensional structure of cyanobacterial photosystem I at 2.5 angstrom resolution. *Nature* **411**, 909-917 (2001).

25. Hofer, R., Textor, M. & Spencer, N.D. Alkyl phosphate monolayers, self-assembled from aqueous solution onto metal oxide surfaces. *Langmuir* **17**, 4014-4020 (2001).

26. Hegner, M., Wagner, P. & Semenza, G. Ultralarge Atomically Flat Template-Stripped Au Surfaces for Scanning Probe Microscopy. *Surf. Sci.* **291**, 39-46 (1993).

27. Mihailetchi, V.D., Blom, P.W.M., Hummelen, J.C. & Rispens, M.T. Cathode dependence of the open-circuit voltage of polymer : fullerene bulk heterojunction solar cells. *J. Appl. Phys.* **94**, 6849-6854 (2003).

28. de Boer, B., Hadipour, A., Mandoc, M.M., van Woudenbergh, T. & Blom, P.W.M. Tuning of metal work functions with self-assembled monolayers. *Adv. Mater.* **17**, 621 (2005).

29. Felder, C.E., Prilusky, J., Silman, I. & Sussman, J.L. A server and database for dipole moments of proteins. *Nucleic Acids Res.* **35**, W512-W521 (2007).

30. Tseng, C.T., Cheng, Y.H. & Lee, M.C.M. Study of anode work function modified by self-assembled monolayers on pentacene/fullerene organic solar cells. *Appl. Phys. Lett.* **91** (2007).

31. Antosiewicz, J. & Porschke, D. Electrostatics of Hemoglobins from Measurements of the Electric Dichroism and Computer-Simulations. *Biophys. J.* **68**, 655-664 (1995).

32. Rippka, R., Deruelles, J., Waterbury, J.B., Herdman, M. & Stanier, R.Y. Generic Assignments, Strain Histories and Properties of Pure Cultures of Cyanobacteria. *J. Gen. Microbiol.* **111**, 1-61 (1979).

33. Mukherjee, D., May, M., Vaughn, M., Bruce, B.D. & Khomami, B. Controlling the Morphology of Photosystem I Assembly on Thiol-Activated Au Substrates. *Langmuir* **26**, 16048-16054 (2010).

34. El-Mohsnawy, E. et al. Structure and Function of Intact Photosystem 1 Monomers from the Cyanobacterium Thermosynechococcus elongatus. *Biochemistry* **49**, 4740-4751 (2010).

35. Porra, R.J., Thompson, W.A. & Kriedemann, P.E. Determination of Accurate Extinction Coefficients and Simultaneous-Equations for Assaying Chlorophyll-a and Chlorophyll-B Extracted with 4 Different Solvents - Verification of the Concentration of Chlorophyll Standards by Atomic-Absorption Spectroscopy. *Biochim. Biophys. Acta.* **975**, 384-394 (1989).